*Article*

# Equilibrium shapes of Ag, Ni, and Ir nanoparticles under CO conditions

**Meng Zhang[1], Yu Han[2,3], Wen Wu Xu[1,*], Beien Zhu[2,4,*] and Yi Gao[2,4]**

1 Department of Physics, School of Physical Science and Technology, Ningbo University, Ningbo 315211, China
2 Shanghai Institute of Applied Physics, Chinese Academy of Sciences, Shanghai 201800, China
3 University of Chinese Academy of Sciences, Beijing 100049, China
4 Interdisciplinary Research Center, Shanghai Advanced Research Institute, Chinese Academy of Sciences, Shanghai 201210, China

**Abstract:** Metal nanoparticles are widely used in catalysis by virtue of their excellent physicochemical properties, which closely related to their morphology. In this work, we predict the reshaping of Ag, Ni, and Ir metal nanoparticles under CO atmosphere by the recently proposed multiscale structure reconstruction model. In the low-pressure environment, temperature has little effect on the structures of Ag nanoparticles. However, the structures of Ag nanoparticles will change significantly in the high-pressure and low-temperature environment. Ni and Ir nanoparticles are greatly affected by environment due to their stronger interactions with CO. This study demonstrates the structural changes of Ag, Ni, and Ir nanoparticles under different pressures and temperatures, providing theoretical guidance for in situ experiments and rational design of nanocatalysts.

**Keywords:** Catalysis; Metal nanoparticle; Reshaping; Multiscale; Reactive condition

## 1. Introduction

Metal nanoparticles (NPs) have gained widespread attention for their ability to improve chemical catalytic performance[1-4]. The size and morphology of NPs have a great influence on their catalytic efficiencies, so there is a great interest in whether and how metal NPs undergo structural changes in the reactive environmen[5-15]. For example, Hansen et al. found the reversible remodeling of Cu NPs under water vapor and CO gas by in situ transmission electron microscopy[14]. Tao et al. observed the dynamic changes in the surface of Rh-Pt alloy NPs under atmospheric conditions of NO and CO by X-ray photoelectron spectroscopy[10]. Tao et al. brought to light that the stepped (557) and (332) faces of Pt crystals have clusters generated on the surface at CO full coverage, a pressure of 1 torr, and room temperature[11]. Recently, Frey et al. found by transmission electron microscopy that Pt NPs undergo remodeling in $H_2$ and $O_2$ atmosphere[5]. It can be seen that great progress has been made in in situ experiments of the structural changes of metal NPs in the reactive environment. Ideally, the in situ studies are necessary for all the potential catalytic systems. However, it can hardly be done in experiments due to the large experimental costs.

Theoretical simulation is, therefore, highly demanded to predict structural changes of metal NPs under different reaction conditions. In the last few years, some theoretical models were proposed to predict the structural changes of nanomaterials under various environmental conditions[16-29]. For example, using Monte Carlo simulations, Cao et al. previously predicted good stability of Mo-doped Pt-Ni alloys under oxidizing conditions[27]. Teck L. Tan et al. used a cluster expansion theory approach to investigate the controlled catalytic application of Pt-Pd alloys in hydrogen precipitation reactions[28].Among these models, multiscale structure reconstruction model (MSR), which was developed based on first-principles calculations, Wulff configurations and thermodynamic adsorption isotherms, has been proved to be a very simple and efficient tool to

quantitatively describe the morphological changes of metal NPs in the gaseous environment. Employing the MSR model, the structural changes of metal NPs (Cu, Au, Pt, and Pd) under water vapor environment were successfully predicted[30]. Besides, the shape evolution of Pd nanoparticles would occur under atmospheric pressure of $O_2$ and $H_2$ [31], which is consistent with the experiment[14]. However, more theoretical predictions of the reshapping behavior of various metal NPs are still needed for the rational design of nanocatalysts.

In this work, we used the MSR model to study the structural reconstruction of Ag, Ni and Ir NPs under CO atmosphere, which are common metal nanocatalysts but have not been studied in previous works. The Ag surfaces have very weak adsorption energy for CO, so the structure remains almost unchanged at low pressures. Ni and Ir have strong adsorption energies for CO, and the structure of NPs changes at even 1 Pa pressure.

## 2. Methodology

### *2.1. DFT calculations*

In this work, all spin-polarized density functional theory (DFT) calculations were performed using the Vienna Ab initio Simulation Package (VASP)[32-34]. The projector-augmented-wave (PAW) was used[35,36]. The cut-off of the plane-wave expansion is 400 eV. The convergence criterion of the electronic self-consistent and the force in a conjugate-gradient algorithm is $10^{-5}$ eV and 0.05 eV/Å, respectively.

The surface energy of three pure metals can be written as

$$E_{surf} = \frac{E_{slab} - NE_{bulk}}{2A} \tag{1}$$

Here, $E_{slab}$ referred to the total energy of a surface periodic slab and $E_{bulk}$ is the energy per atom of the bulk metal, $A$ denoted the area of the slab and $N$ is the number of the pure metal atoms in the slab.

For CO adsorption calculations, Perdew-Burke-Ernzerhof (PBE) functional for Ag [37]and revised form of the PBE functional (RPBE) for Ni and Ir were employed[38,39]. For the (4×4) slab, creating a 6-layer atomic layer with a vacuum of 20 Å. The K points [40,41] of the (4×4) and (1×1) slabs were set as (8×8×1). Considering the repulsive effect when adsorption of CO on the surface, we calculated the adsorption energies of CO using the (1×1) slab for 100% coverage, and the adsorption energies of single CO molecules in the (4×4) slab to get the repulsive energy $\omega$.

Then, the $\omega$ for CO can be written as

$$\omega = \frac{E_{ads} - E_{ads(1\times1)}}{z} \tag{2}$$

Here, $E_{ads}$ is the adsorption energy of a single CO on the (4×4) slab, and $E_{ads(1\times1)}$ is the molecular adsorption energy at (1×1) slab, and $z$ is number of nearest neighbor surface coordination atoms.

When CO at the surfaces, the entropy $S_{ads}$ is set to 0. The entropy of gas-phase molecules $S_{gas}$ is described by

$$S = S(T, P^0) - R\ln(\frac{P}{P^0}) \tag{3}$$

Here, $P^0$ is 1 atm, and $S(T, P^0)$ is entropy at 1 atm with different temperature. The $S(T, P^0)$ is fitted by data from the NIST-JANAF Thermochemical Tables[42].

### *2.2. MSR model*

MSR is a multiscale model recently proposed that nanoclusters are reconfigured under atmospheric conditions. This model is composed of the Wulff construction, thermodynamic isotherms, and first-principle calculations.

Under CO gas environment, the interface tension can be modified as

$$\gamma_{hkl}^{int} = \gamma_{hkl} + \theta\left(\frac{E_{ads}}{A_{at}}\right) \quad (4)$$

Here, $E_{ads}$ is adsorption energy of the CO molecule, $\theta$ means the surface coverage by the adsorbed CO molecules, and $A_{at}$ is the surface area per surface atom. The surface coverage $\theta$ is decided by CO pressure (P), temperature (T), and the adsorption energy ($E_{ads}$). Considering the interaction of adsorbed CO on the metal surface we changed Eq. (4) to Eq. (5) as:

$$\gamma_{hkl}^{int} = \gamma_{hkl} + \frac{\theta(E_{ads} - zw\theta)}{A_{at}} \quad (5)$$

Then, $\theta$ can be calculated by the Fowler-Guggenheim (F-G) adsorption isotherm, where the lateral interaction between adsorbed CO is assumed to have a linear relationship to $\theta$. This assumption works very well for low-index surfaces, but more test calculations concerning the adsorption configurations are needed when applying this model on high-index surfaces [43]:

$$PK = \frac{\theta}{1-\theta}e^{-c\theta} \quad (6)$$

$$c = \frac{zw}{RT} \quad (7)$$

Here, R means the gas constant, K is the adsorption equilibrium constant, which can be written as

$$K = \exp\left(\frac{-\Delta G}{RT}\right) = \exp\left(\frac{-E_{ads} + T\left(S_{ads} - S_{gas}\right)}{RT}\right) \quad (8)$$

Where $S_{ads}$ is the entropy of adsorbed CO molecule, and $S_{gas}$ is the entropy of adsorbed gas-phase CO molecule.

## 3. Results and discussions

Table 1 shows the surface energy of the three metals and surface area per atom of three low-index surfaces for single Ag, Ni and Ir NPs. Table 2 presents the adsorption energy of CO for three metals on three low-index surfaces and CO repulsion energy on metal surfaces. As shown in Table 2, The adsorption behavior of CO is different for different metals and different surfaces. The adsorption energy of CO on Ag is very weak compared to Ni and Ir, so the repulsion energy of CO on the surface of Ag is also very weak.

In order to understand the reconfiguration of Ag, Ni and Ir NPs in CO atmosphere, their equilibrium structures are shown in Figs. 1-3. Ag, Ni and Ir are all Face-Centered Cubic (FCC) structures, and the size of their models is about 5 nm. The simulated temperatures are 300 K to 900 K and the pressures are 1 Pa, 100 Pa, and 1 bar, respectively. Figs. 4-6 shows the variation of CO coverage and surface energy with temperature for three low index surfaces of the equilibrium structure of NPs, corresponding to Figs. 1-3, respectively.

**Table 1.** The surface energies (eV/ Å$^2$) and surface area per atom $A_{at}$(Å$^2$) of three metals.

| | **100** | | **110** | | **111** | |
|---|---|---|---|---|---|---|
| | Surface energy | $A_{at}$ | Surface energy | $A_{at}$ | Surface energy | $A_{at}$ |
| Ag | 0.05 | 8.35 | 0.06 | 11.80 | 0.05 | 7.23 |
| Ni | 0.14 | 6.21 | 0.14 | 8.78 | 0.09 | 5.38 |
| Ir | 0.17 | 7.37 | 0.18 | 10.42 | 0.14 | 6.38 |

**Table 2.** Adsorption energy $E_{ads}$(eV) of CO molecules on three metals, and repulsion energy between adsorbates $w$(eV) are presented.

| | 100 | | 110 | | 111 | |
|---|---|---|---|---|---|---|
| | $E_{ads}$ | $w$ | $E_{ads}$ | $w$ | $E_{ads}$ | $w$ |
| Ag | -0.23 | -0.05 | -0.34 | -0.06 | -0.16 | -0.05 |
| Ni | -1.53 | -0.27 | -1.54 | -0.21 | -1.61 | -0.27 |
| Ir | -1.89 | -0.18 | -2.12 | -0.17 | -1.74 | -0.22 |

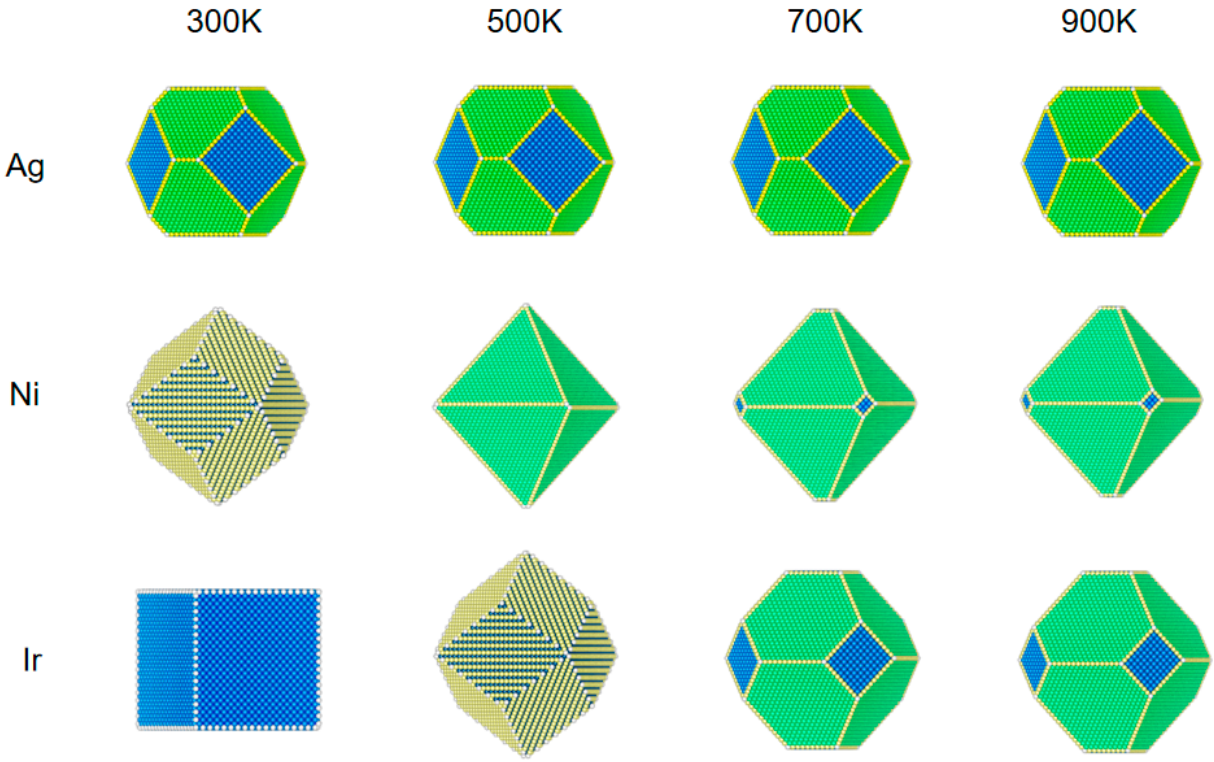


**Figure 1.** The structural evolution of 5 nm metal NPs (Ag, Ni ,Ir) at different temperatures and 1 Pa of CO. Blue is 100 surface, yellow is 110 surface and green is 111 surface.

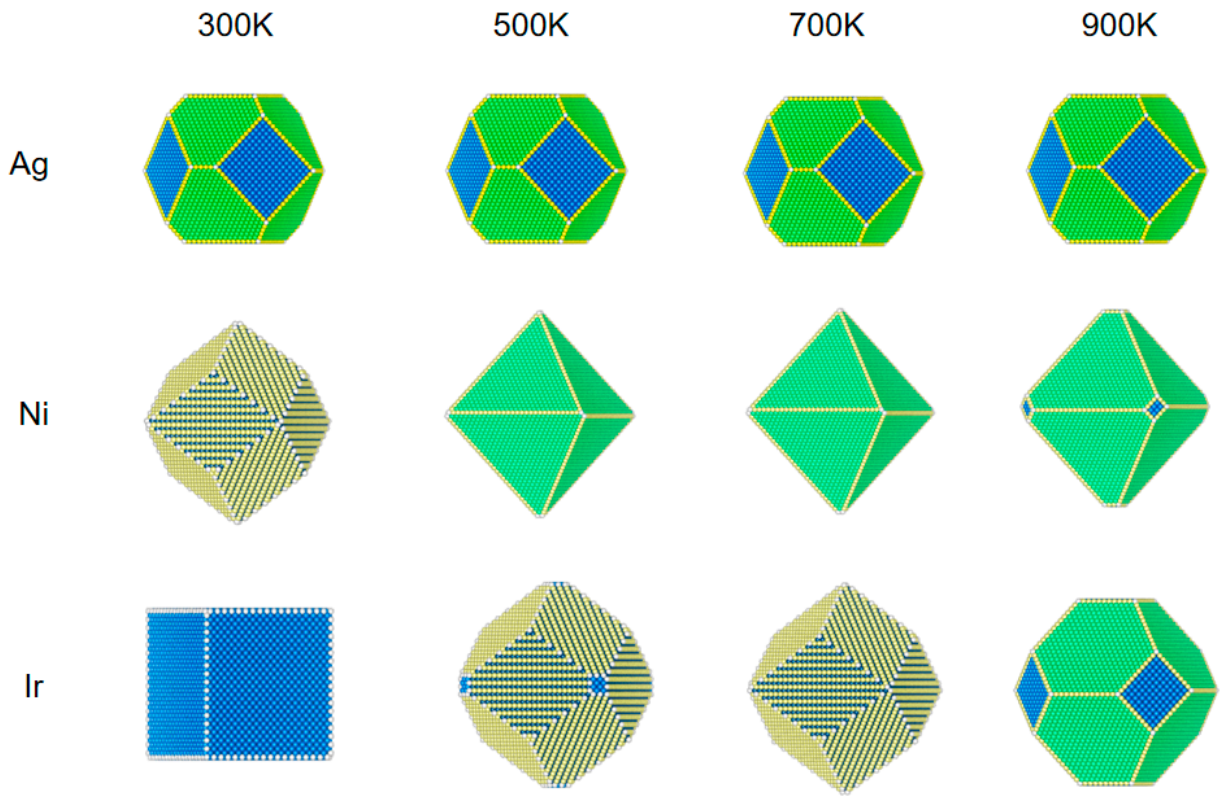


**Figure 2.** The structural evolution of 5 nm metal NPs (Ag, Ni ,Ir) at different temperatures and 100 Pa of CO.

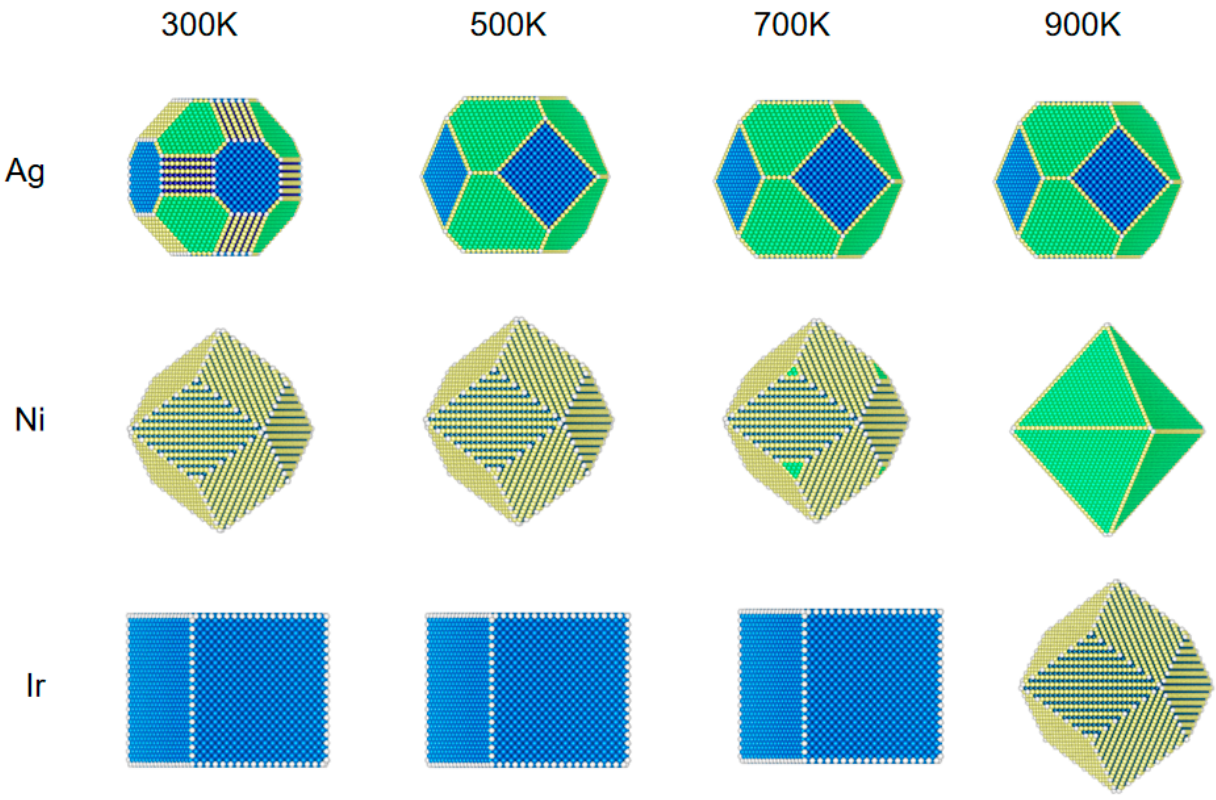


**Figure 3.** The structural evolution of 5 nm of metal NPs (Ag, Ni ,Ir) at different temperatures and 1 bar of CO.

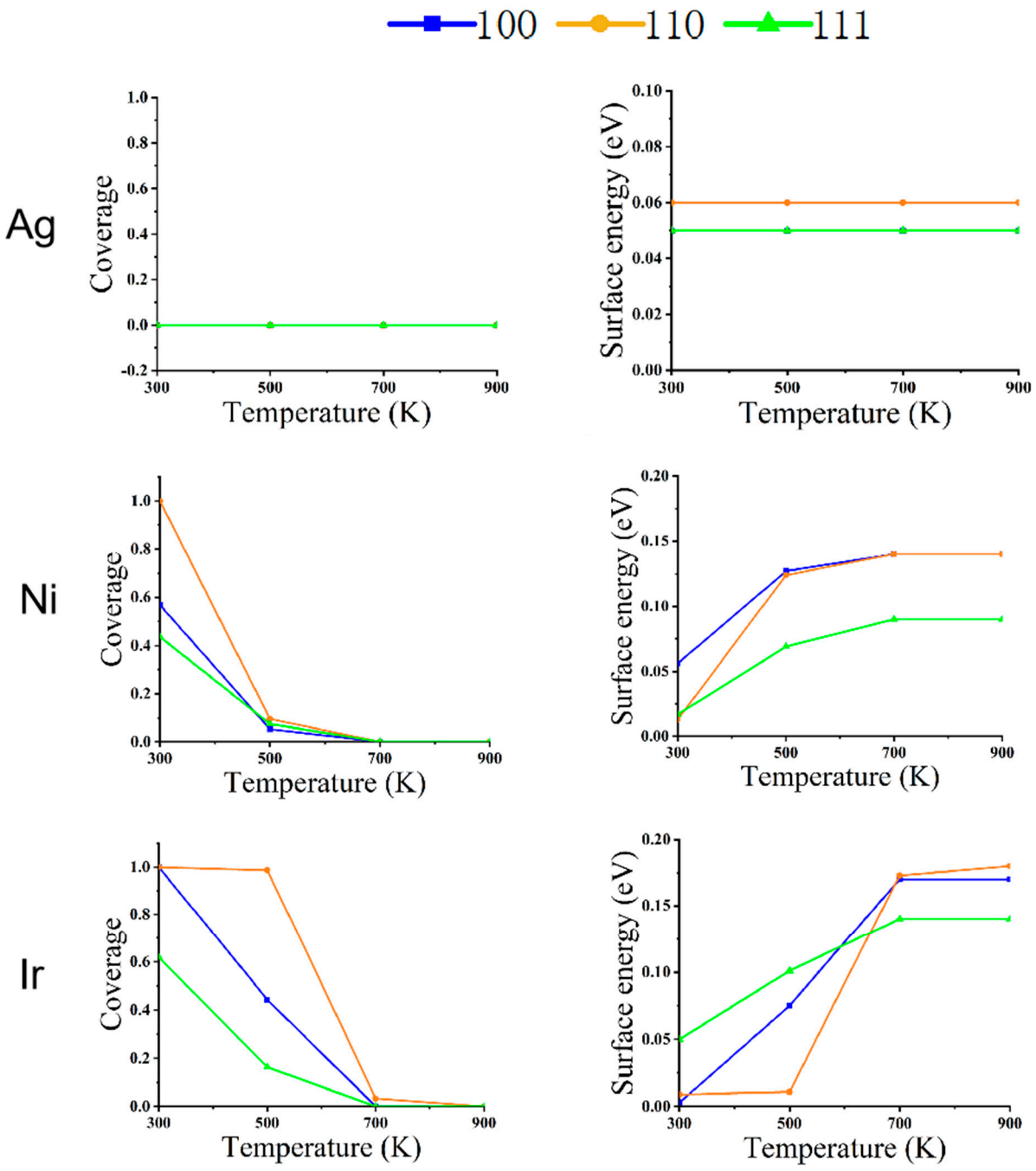


**Figure 4.** The relationship between the coverage of CO (left) and surface energy (right) in different faces of metal NPs (Ag, Ni, Ir) at changing temperature and pressure 1 Pa.

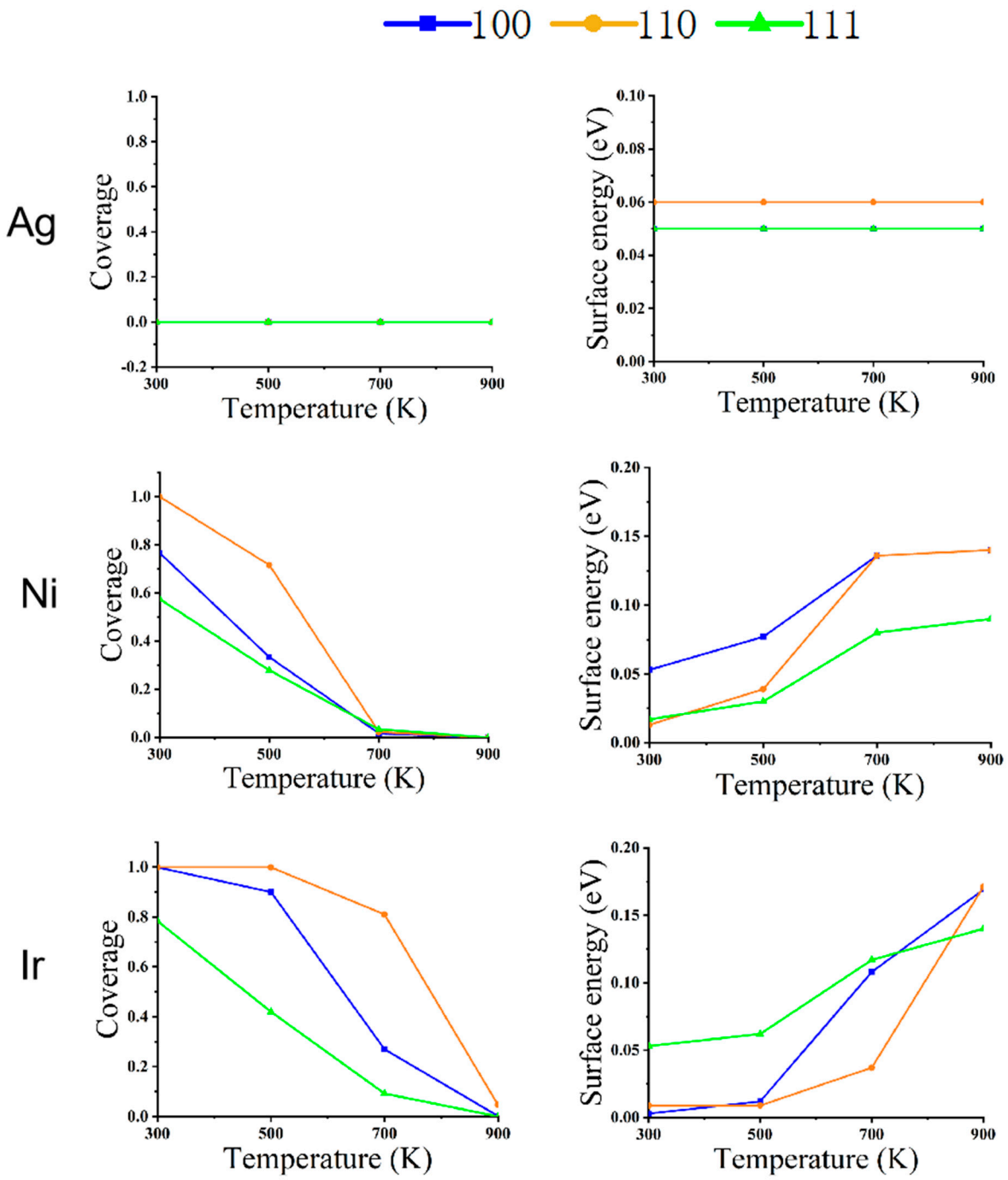


**Figure 5.** The relationship between the coverage of CO (left) and surface energy (right) in different faces of metal NPs (Ag, Ni ,Ir) at changing temperature and pressure 100 Pa .

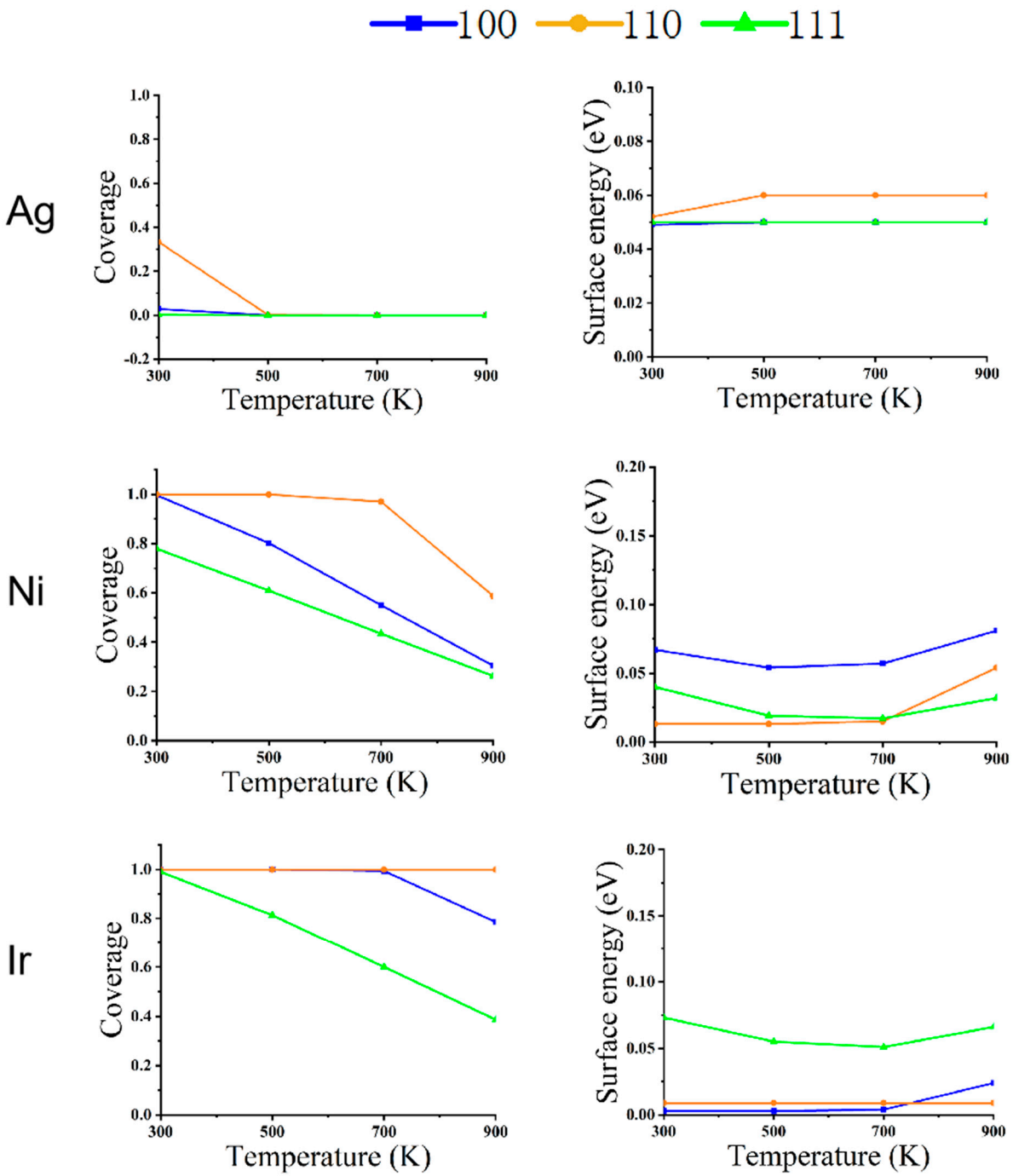


**Figure 6.** The relationship between the coverage of CO (left) and surface energy (right) in different faces of metal NPs (Ag, Ni ,Ir) at changing temperature and pressure 1 bar.

As shown in Fig. 1, Ag NPs at the pressure of 1 Pa, the equilibrium structure does not change with temperature under CO atmosphere. As can be seen from Figure 4, there is no CO adsorption on the surface due to the weak adsorption energy of CO on Ag and surface energy of (100), (110), and (111) faces don't change, even at a low temperature of 300 K.

Ni NPs show significant structural changes at a the pressure of 1 Pa. At 300K, CO coverage on (110) is 100%, (100) is 57%, and (111) is 44%. Since the repulsion energy of CO on the (110) surface is minimal for the other two surfaces, the equilibrium structures of Ni NPs are all rhombic dodecahedra composed of the (110) surface. When the temperature increases from 300 K to 500 K, the CO adsorption on the three low index surfaces decreases rapidly to near zero. The (111) surface has the smallest surface energy relative to the (100)

and (110) surfaces, so the structure of the NPs changes from a rhombic dodecahedron to an octahedron composed entirely of the (111) surface. When the temperature rises to 700 K, there is no adsorption of CO on the three low index surfaces and the equilibrium structure becomes a truncated octahedron with the truncated part being the (100) surface. When the temperature increases from 700K to 900K the nanoparticle structure does not change.

We can observe that the structural changes of Ir NPs are also different from Ni NPs. The coverage of CO adsorption at (100) and (110) is 100% at 300 K, but the (100) surface has a lower surface energy compared to the (110) surface, under this condition the Ir NPs form a cube consisting of (100) faces. When the temperature rises to 500 K, CO coverage at (100) decreases to 44% at (110) with 99% coverage, at this point (110) has a very low surface energy with respect to (100) and (111), and a cube becomes a rhombic dodecahedron. When the temperature rises from 500 K to 700 K, the CO coverage in (110) decreases to 17% about the same as in (100) and (111). As the temperature rises from 500 K to 700 K, CO coverage decreases to 3% at (110) and 0 at (100) and (111). Thus, a rhombic dodecahedron becomes a truncated octahedron. When the temperature is increased from 700K to 900K, there is little effect on Ir NPs, so the equilibrium structure does not change. When the interaction with CO is strong, Ir NPs expose only the (100) surface. As the mutual CO interaction with the surface decreases, only the truncated octahedra consisting of (100) and (111) are exposed, this is similar to the recent report[44].

Fig. 2. gives the structures of the three NPs at a pressure of 100 Pa. For Ag NPs, changing the temperature at a pressure of 100 Pa has almost no effect on its structure.

The structural reconstruction of Ni NPs is similar to 1 Pa at a pressure of 100 Pa. At 700 K, all three low index surfaces have 2% CO coverage, which is not the same as a pressure of 1 Pa is no CO coverage. The NPs become an octahedral equilibrium structure.

Because of the high adsorption energy and low repulsion energy of Ir NPs for CO, the equilibrium structure also changes significantly compared to the pressure of 1 Pa. When the temperature is 600 K, the coverage of (100) adsorbed CO is 90%, at this time (100) also has a low surface energy, and the rhombic dodecahedron has a cut-off angle generated by the composition of (100). As the temperature increases from 600K to 800K, (100) drops to 27% coverage for CO, and (110) is still 81% high coverage. The surface energy of (110) is very low relative to (100) and (111). The nanostructure changes from a truncated dodecahedron to a rhombic dodecahedron. When the temperature rises to 900 K, the CO coverage on all surfaces is essentially 0. The structure changes from a rhombic dodecahedron to a truncated octahedron.

As can be seen from Fig. 3, Ag NPs at a pressure of 1 bar CO temperature of 300 K are different from low pressure 1 Pa and 100 Pa. At 300 K, CO coverage is 33% at (110) and 3% at (100). The fraction of (110) increases more rapidly than (100) and (110). Due to the high pressure, the Ni and Ir surfaces are more strongly adsorbed to CO, so the structures until 700 K of temperature are similar to those at 300 K. In particular, Ir NPs are still 100% CO coverage at 900 K (110). The surface of Ni also has adsorption also differs from the low-pressure case.

Figures 4 to 6 depict the variation of CO coverage and surface energy on the low-index surface of metal nanoparticles at different temperature pressure. With increasing pressure, the coverage of all three low index surfaces of Ni and Ir increases significantly up to 700 K for CO Increasing from 100 pa to 1 bar, the rate of change of CO coverage also increases significantly due to the large pressure change.Figure 6 shows that in the high pressure environment, the surface energy of the three metals is lower relative to the low

pressure environment surface energy. Also, the three low index surface energies are not positively correlated with temperature as in Figs. 4 and 5.

Fig. 7 shows the percentage of low index surfaces for Ag, Ni and Ir at different pres sures and temperatures. Coordination numbers less than 7 are defined as edge and corner atoms. We note that there are more edge and corner atoms when the NPs expose more (100) and (110) facets. These structures may have better catalytic properties since the low-coordinated sites are normally more active than the high-coordinated ones. The (110) surface has a lower coordination number with respect to (100) and (111). We can see a significant increase in the (110) surface of Ag at a high pressure of 1 bar at a temperature of 300 K. At a high pressure of 1 bar, the Ni NPs also have a large (110) fraction before 700 K. For Ir NPs, (100) also has high coverage on CO and (100) will form a lower surface energy than (110) and (111). So Ir NPs are prone to equilibrium structure at low temperatures into a cube consisting of (100). For Ag NPs at a pressure of 1 bar temperature of 300 K, the surface energy of (110) surface decreases, so (110) can be seen significantly increased in the figure. For Ni NPs at pressures of 1 Pa and 100 Pa, the (111) surface usually has a lower surface energy than the other two surfaces, so the structure is more exposed to the (111) surface. The pressure increases to 1 bar, (110) has a more stable surface energy, so more of the (110) surface is exposed. For Ir NPs, the more exposed surfaces also have lower surface energy relative to other surfaces in a given environment.

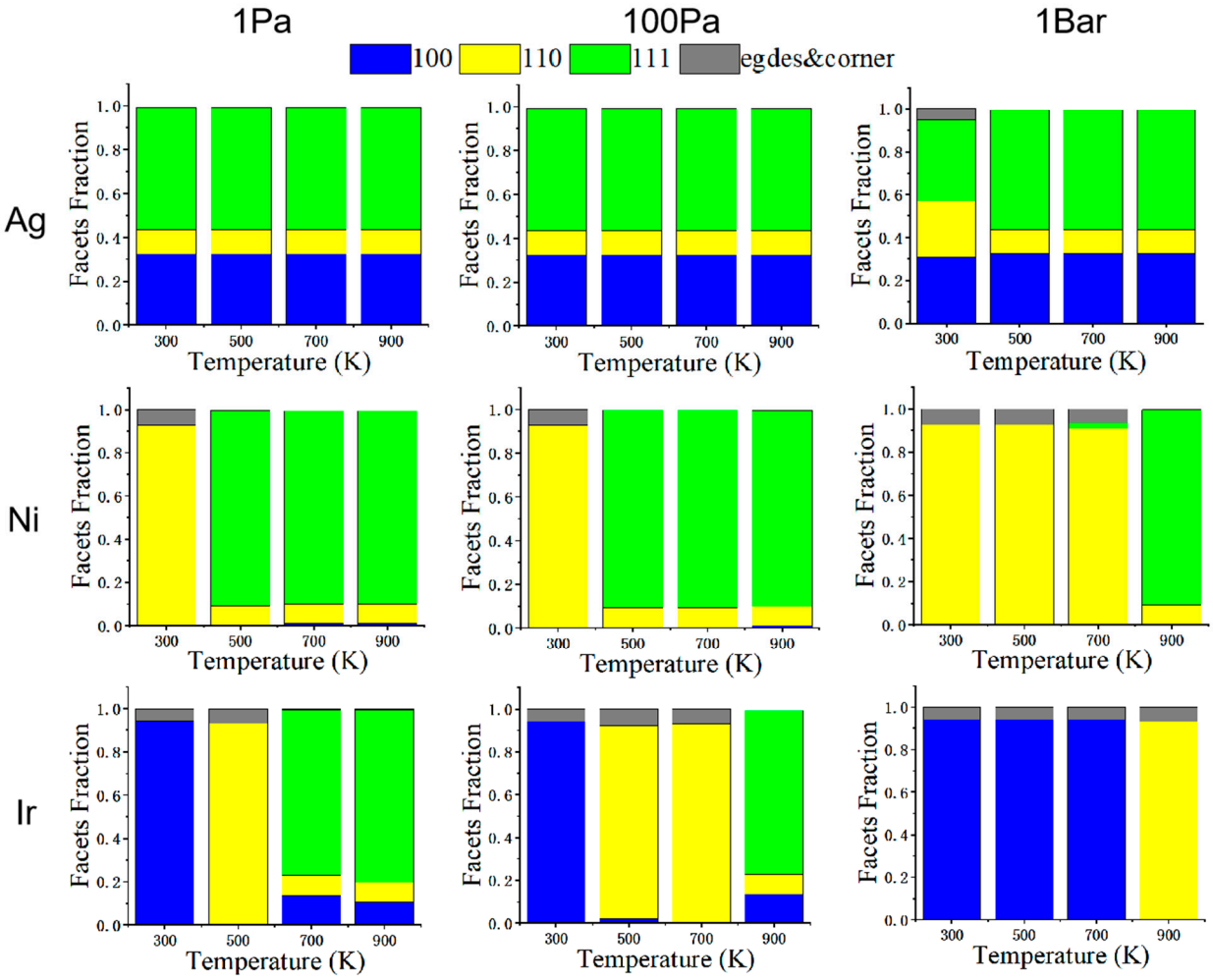


**Figure 7.** The fraction of (100), (110) and (111) facets of corresponding structures under three pressures (1Pa, 100Pa and 1bar). Egdes&corner is the part of the coordination number less than 7.

## 4. Conclusions

In this work, we propose a multiscale reconstruction model based on gas adsorption interaction. The MSR model is used to predict the equilibrium structures of different metal NPs (Ag, Ni, Ir) at different temperature pressures under CO atmosphere. In particular, the weak adsorption energy of CO on the Ag surface, the (110) surface of the equilibrium structure increases at high pressure (1 bar) and low temperature (300 K). Under the same conditions, the coverage of the (110) surface is higher than that of the (100) and (111) surfaces due to the effect of the adsorption and repulsion energies of CO. Since the coordination number of (111) surface is higher than that of (100) and (110), this part of (111) increases sharply on the nanoparticle surface as the CO coverage decreases. This work provides a more comprehensive understanding for in situ experiments and theoretical guidance for the rational design of nanocatalysts (Ag, Ni, Ir).

## References

1. Liao, H.G.; Jiang, Y.X.; Zhou, Z.Y.; Chen, S.P.; Sun, S.G. Shape-controlled synthesis of gold nanoparticles in deep eutectic solvents for studies of structure–functionality relationships in electrocatalysis. *Angewandte Chemie International Edition* **2008**, *47*, 9100-9103.
2. Narayanan, R.; El-Sayed, M.A. Catalysis with transition metal nanoparticles in colloidal solution: nanoparticle shape dependence and stability. *The Journal of Physical Chemistry B* **2005**, *109*, 12663-12676.

3. Burda, C.; Chen, X.; Narayanan, R.; El-Sayed, M.A. Chemistry and properties of nanocrystals of different shapes. *Chemical reviews* **2005**, *105*, 1025-1102.
4. Ahmadi, T.S.; Wang, Z.L.; Green, T.C.; Henglein, A.; El-Sayed, M.A. Shape-controlled synthesis of colloidal platinum nanoparticles. *Science* **1996**, *272*, 1924-1925.
5. Frey, H.; Beck, A.; Huang, X.; van Bokhoven, J.A.; Willinger, M.-G. Dynamic interplay between metal nanoparticles and oxide support under redox conditions. *Science* **2022**, *376*, 982-987.
6. Abuin, M.; Kim, Y.Y.; Runge, H.; Kulkarni, S.; Maier, S.; Dzhigaev, D.; Lazarev, S.; Gelisio, L.; Seitz, C.; Richard, M.-I. Coherent X-ray imaging of CO-adsorption-induced structural changes in Pt nanoparticles: implications for catalysis. *ACS Applied Nano Materials* **2019**, *2*, 4818-4824.
7. Avanesian, T.; Dai, S.; Kale, M.J.; Graham, G.W.; Pan, X.; Christopher, P. Quantitative and atomic-scale view of CO-induced Pt nanoparticle surface reconstruction at saturation coverage via DFT calculations coupled with in situ TEM and IR. *Journal of the American Chemical Society* **2017**, *139*, 4551-4558.
8. Jiang, Y.; Li, H.; Wu, Z.; Ye, W.; Zhang, H.; Wang, Y.; Sun, C.; Zhang, Z. In situ observation of hydrogen-induced surface faceting for palladium–copper nanocrystals at atmospheric pressure. *Angewandte Chemie International Edition* **2016**, *55*, 12427-12430.
9. Baldi, A.; Narayan, T.C.; Koh, A.L.; Dionne, J.A. In situ detection of hydrogen-induced phase transitions in individual palladium nanocrystals. *Nature materials* **2014**, *13*, 1143-1148.
10. Yuan, Y.; Yan, N.; Dyson, P.J. Advances in the rational design of rhodium nanoparticle catalysts: control via manipulation of the nanoparticle core and stabilizer. *Acs Catalysis* **2012**, *2*, 1057-1069.
11. Tao, F.; Salmeron, M. In situ studies of chemistry and structure of materials in reactive environments. *Science* **2011**, *331*, 171-174.
12. Tao, F.; Grass, M.E.; Zhang, Y.; Butcher, D.R.; Renzas, J.R.; Liu, Z.; Chung, J.Y.; Mun, B.S.; Salmeron, M.; Somorjai, G.A. Reaction-driven restructuring of Rh-Pd and Pt-Pd core-shell nanoparticles. *Science* **2008**, *322*, 932-934.
13. Liu, Z.; Ihl Woo, S. Recent advances in catalytic DeNOx science and technology. *Catalysis Reviews* **2006**, *48*, 43-89.
14. Hansen, P.L.; Wagner, J.B.; Helveg, S.; Rostrup-Nielsen, J.R.; Clausen, B.S.; Topsøe, H. Atom-resolved imaging of dynamic shape changes in supported copper nanocrystals. *Science* **2002**, *295*, 2053-2055.
15. Tao, A.R.; Habas, S.; Yang, P. Shape control of colloidal metal nanocrystals. *small* **2008**, *4*, 310-325.
16. Yuan, L.; Li, X.; Zhu, B.; Zhang, G.; Gao, Y. Reshaping of Rh nanoparticles in operando conditions. *Catalysis Today* **2020**, *350*, 184-191.
17. Rossi, K.; Asara, G.G.; Baletto, F. A genomic characterisation of monometallic nanoparticles. *Physical Chemistry Chemical Physics* **2019**, *21*, 4888-4898.
18. Chepkasov, I.; Visotin, M.; Kovaleva, E.; Manakhov, A.; Baidyshev, V.; Popov, Z. Stability and electronic properties of PtPd nanoparticles via MD and DFT calculations. *The Journal of Physical Chemistry C* **2018**, *122*, 18070-18076.
19. Nanba, Y.; Ishimoto, T.; Koyama, M. Structural stability of ruthenium nanoparticles: a density functional theory study. *The Journal of Physical Chemistry C* **2017**, *121*, 27445-27452.
20. Zhu, B.; Creuze, J.; Mottet, C.; Legrand, B.; Guesmi, H. CO adsorption-induced surface segregation and formation of Pd chains on AuPd (100) alloy: Density Functional Theory based Ising model and Monte Carlo simulations. *The Journal of Physical Chemistry C* **2016**, *120*, 350-359.
21. Turner, C.H.; Lei, Y.; Bao, Y. Modeling the atomistic growth behavior of gold nanoparticles in solution. *Nanoscale* **2016**, *8*, 9354-9365.

22. Wang, Y.-G.; Yoon, Y.; Glezakou, V.-A.; Li, J.; Rousseau, R. The role of reducible oxide–metal cluster charge transfer in catalytic processes: new insights on the catalytic mechanism of CO oxidation on Au/TiO2 from ab initio molecular dynamics. *Journal of the American Chemical Society* **2013**, *135*, 10673-10683.
23. Ouyang, R.; Liu, J.-X.; Li, W.-X. Atomistic theory of Ostwald ripening and disintegration of supported metal particles under reaction conditions. *Journal of the American Chemical Society* **2013**, *135*, 1760-1771.
24. Zafeiratos, S.; Piccinin, S.; Teschner, D. Alloys in catalysis: phase separation and surface segregation phenomena in response to the reactive environment. *Catalysis Science & Technology* **2012**, *2*, 1787-1801.
25. Barmparis, G.D.; Remediakis, I.N. Dependence on CO adsorption of the shapes of multifaceted gold nanoparticles: A density functional theory. *Physical Review B* **2012**, *86*, 085457.
26. Li, C.; Raciti, D.; Pu, T.; Cao, L.; He, C.; Wang, C.; Mueller, T. Improved prediction of nanoalloy structures by the explicit inclusion of adsorbates in cluster expansions. *The Journal of Physical Chemistry C* **2018**, *122*, 18040-18047.
27. Cao, L.; Mueller, T. Theoretical insights into the effects of oxidation and Mo-doping on the structure and stability of Pt–Ni nanoparticles. *Nano Letters* **2016**, *16*, 7748-7754.
28. Tan, T.L.; Wang, L.-L.; Johnson, D.D.; Bai, K. A comprehensive search for stable Pt–Pd nanoalloy configurations and their use as tunable catalysts. *Nano letters* **2012**, *12*, 4875-4880.
29. Yuge, K. Segregation of Pt28Rh27 bimetallic nanoparticles: a first-principles study. *Journal of Physics: Condensed Matter* **2010**, *22*, 245401.
30. Zhu, B.; Xu, Z.; Wang, C.; Gao, Y. Shape evolution of metal nanoparticles in water vapor environment. *Nano letters* **2016**, *16*, 2628-2632.
31. Zhang, X.; Meng, J.; Zhu, B.; Yu, J.; Zou, S.; Zhang, Z.; Gao, Y.; Wang, Y. In situ TEM studies of the shape evolution of Pd nanocrystals under oxygen and hydrogen environments at atmospheric pressure. *Chemical Communications* **2017**, *53*, 13213-13216.
32. Kresse, G.; Furthmüller, J. Efficiency of ab-initio total energy calculations for metals and semiconductors using a plane-wave basis set. *Computational materials science* **1996**, *6*, 15-50.
33. Kresse, G.; Furthmüller, J. Efficient iterative schemes for ab initio total-energy calculations using a plane-wave basis set. *Physical review B* **1996**, *54*, 11169.
34. Kresse, G.; Hafner, J. Ab initio molecular dynamics for liquid metals. *Physical review B* **1993**, *47*, 558.
35. Kresse, G.; Joubert, D. From ultrasoft pseudopotentials to the projector augmented-wave method. *Physical review b* **1999**, *59*, 1758.
36. Blöchl, P.E. Projector augmented-wave method. *Physical review B* **1994**, *50*, 17953.
37. Patra, A.; Peng, H.; Sun, J.; Perdew, J.P. Rethinking CO adsorption on transition-metal surfaces: Effect of density-driven self-interaction errors. *Physical Review B* **2019**, *100*, 035442.
38. Gajdoš, M.; Hafner, J.; Eichler, A. Ab initio density-functional study of NO on close-packed transition and noble metal surfaces: I. Molecular adsorption. *Journal of Physics: Condensed Matter* **2005**, *18*, 13.
39. Gajdoš, M.; Eichler, A.; Hafner, J. CO adsorption on close-packed transition and noble metal surfaces: trends from ab initio calculations. *Journal of Physics: Condensed Matter* **2004**, *16*, 1141.
40. Blöchl, P.E.; Jepsen, O.; Andersen, O.K. Improved tetrahedron method for Brillouin-zone integrations. *Physical Review B* **1994**, *49*, 16223.
41. Monkhorst, H.J.; Pack, J.D. Special points for Brillouin-zone integrations. *Physical review B* **1976**, *13*, 5188.
42. Chase Jr, M.W. JANAF thermochemical table. *J. Phys. Chem. Ref. Data* **1985**, *14*, Supplement No. 1.
43. Fowler, R.H.; Guggenheim, E.A. Statistical thermodynamics. *Cambridge University Press: Cambridge* **1939**, pp 431-450.

44. Assaf, N.W.; Suleiman, I.A.; Shawaqfeh, A.T. The surface energy phase diagrams of CO adsorption on the low index iridium surfaces and the morphology of iridium nanoparticles. *Journal of Crystal Growth* **2022**, *593*, 126774.